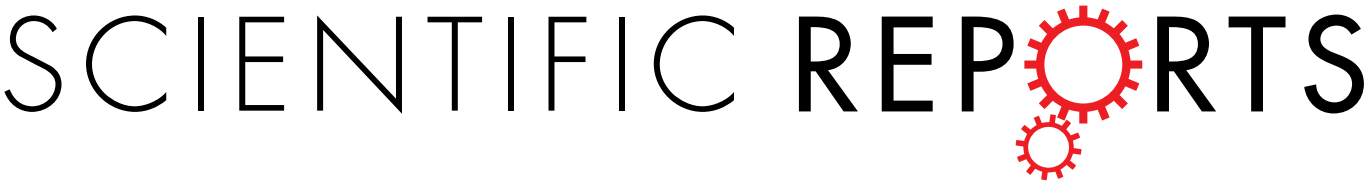

OPEN

Critical field enhancement of asymptotic optical bound states in the continuum

Received: 24 September 2015
Accepted: 16 November 2015
Published: 17 December 2015

Jae Woong Yoon[1,‡], Seok Ho Song[2] & Robert Magnusson[1]

We study spectral singularities and critical field enhancement factors associated with embedded photonic bound states in subwavelength periodic Si films. Ultrahigh-Q resonances supporting field enhancement factor exceeding 10^8 are obtained in the spectral vicinity of exact embedded eigenvalues in spite of deep surface modulation and vertical asymmetry of the given structure. Treating relations between the partial resonance Q and field enhancement factors with an analytical coupled-mode model, we derive a general strategy to maximize the field enhancement associated with these photonic bound states in the presence of material dissipation. The analytical expression for the field enhancement quantitatively agrees with rigorous numerical calculations. Therefore, our results provide a general knowledge for designing practical resonance elements based on optical bound states in the continuum in various applications.

High-Q optical resonances in periodic thin films are connected conceptually to embedded bound states which do not reradiate external waves. These were originally proposed in hypothetical quantum systems by von Neumann and Wigner[1]. In such systems, a completely bound state exists at an energy level above the lowest continuum level. Marinica *et al.* proposed a symmetric double-grating structure to support embedded photonic bound states by coupling between two identical resonant grating layers[2]. Hsu *et al.* experimentally showed a diverging radiation Q factor as a signature of embedded bound states in a single layer of a freestanding Si_3N_4 thin-film photonic crystal[3]. More recently, complete 3-dimensional optical confinement in open scattering systems was suggested using layered plasmonic nanoparticles[4,5].

In real optical systems, embedded bound states are excited or probed in an asymptotic manner[3,6] since at the exact condition they do not interact with the continuum states that contribute to the observation in the far field. In other words, what we actually measure in the laboratory is the resonance response of leaky modes that asymptotically approach a targeted bound state creating a virtual singularity in the spectrum. In this aspect, an important question concerns the properties of the resonance Q factor (Q) as the configuration approaches the exact bound state condition. A related point is the maximal achievable field enhancement. Obviously, field enhancement or excitation strength does not simply increase with diverging Q because the mode excitation vanishes at the exact point of $Q = \infty$ as long as no significant non-linear coupling occurs between the bound state and the external continuum[7]. Therefore, there must exist an optimum quasi-embedded bound-state resonance configuration somewhere in-between highly leaky and completely trapped mode conditions. This is a crucial problem for sensing, nonlinear applications, and cavity-QED problems. Nevertheless, this issue has not been discussed in detail to date. Importantly, leaky-mode resonance with intermediate Q and associated strong field enhancement is currently of high interest as they have versatile properties enabling high-performance optical filters[8], label-free biosensors[9], lossless mirrors[10], dielectric metasurfaces[11,12], dielectric-based optical magnetism[13], and many others[14,15].

In this paper, we study resonance Q factors and field enhancement effects originating in embedded photonic bound states in periodic Si thin-film structures. We show that a 700-nm-thick fully etched Si thin-film grating supports a symmetry-protected bound state at zero in-plane wave vector ($k_{||} = 0$) with ultrahigh resonance Q and electric field intensity enhancement factors exceeding 10^8. The same structure also supports a quasi-embedded bound state at $k_{||} \neq 0$ in spite of vertical asymmetry of the structure. Field enhancement factors of these photonic resonances show a non-trivial relation with the resonance Q factors in the presence of absorption. We explain this

[1]Department of Electrical Engineering, University of Texas - Arlington, Box 19016, Arlington, TX 76019, USA. [2]Department of Physics, Hanyang University, Seoul, 133-791, KOREA. [‡]Present address: Department of Physics, Hanyang University, KOREA. Correspondence and requests for materials should be addressed to S.H.S. (email: shsong@hanyang.ac.kr)

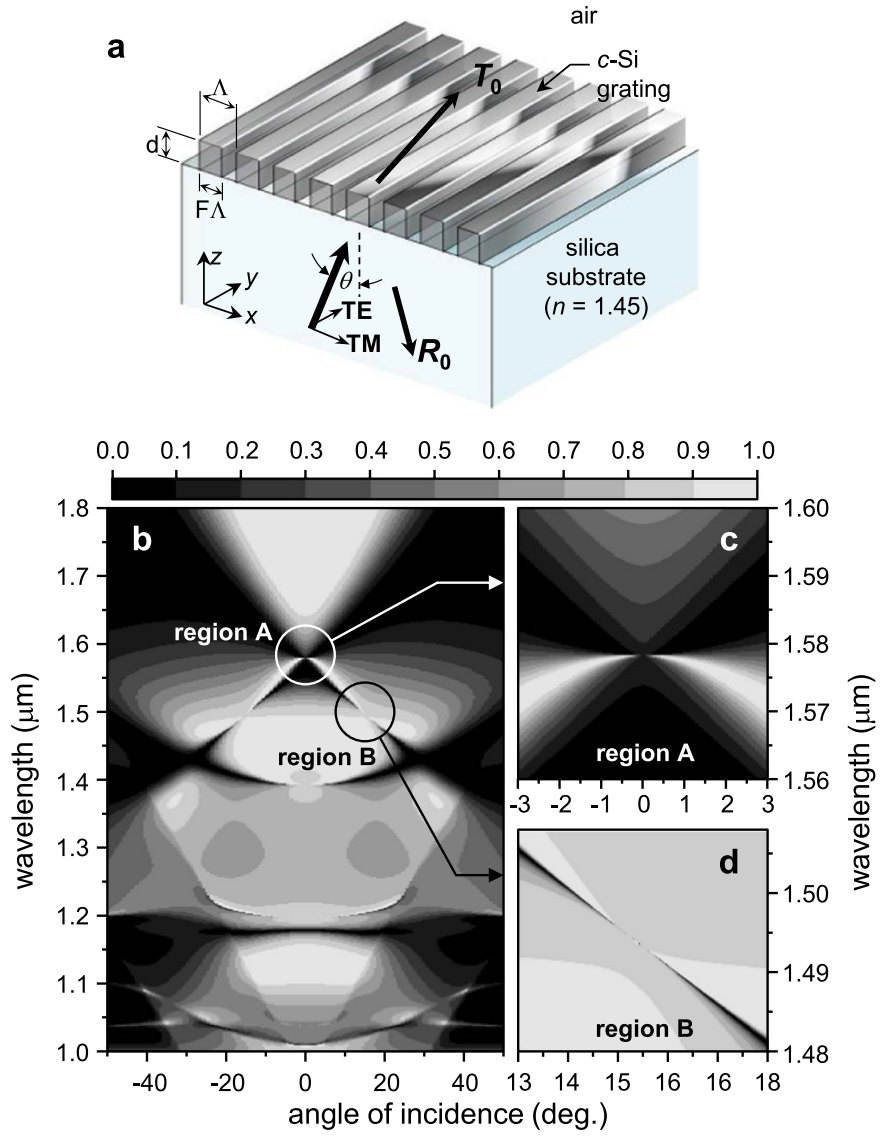

Figure 1. Geometry of the problem and spectral response of an exemplary structure. (**a**) Schematic of a high-Q resonance element consisting of a fully etched crystalline Si (*c*-Si) grating on SiO_2 substrate. (**b–d**) Optical response of a *c*-Si thin-film grating with $\Lambda = 660$ nm, F = 0.7, and d = 700 nm under TM-polarized light incidence. (**b**) Zero-order transmittance (T_0) as a function of wavelength and angle of incidence. (**c**,**d**) show magnified T_0 maps for regions A and B, respectively.

relation with an analytic theory based on the coupled-mode theory of optical Fano resonances. As a crucial factor for applying this device class to practical applications, we discuss methods to maximize resonance Q factors for a given, unavoidable level of material dissipation.

Spectral and angular properties

We consider a subwavelength periodic thin-film structure consisting of a crystalline Si grating with period Λ, fill factor F, and thickness d between an air half space and a silica substrate ($n_{sub} = 1.45$) as shown in Fig. 1a. Polarization of the incident optical field is defined in reference to the plane of incidence: transverse electric (TE) polarization for the electric field perpendicular to the plane of incidence and transverse magnetic (TM) polarization for the magnetic field perpendicular to the plane of incidence. θ denotes the angle of incidence. We use the rigorous coupled-wave analysis[16] for numerical calculation of the spectral response and associated internal field properties. We model the crystalline Si with frequency dispersive complex refractive index $n_{Si}(\lambda) = n_R(\lambda) + ik_I(\lambda)$ and use n_R and k_I values listed in[17].

Figure 1b shows the angle-dependent zero-order transmission (T_0) spectrum through a c-Si thin-film grating with $\Lambda = 660$ nm, F = 0.7, and d = 700 nm under TM-polarized plane-wave incidence. The T_0 spectrum shows broad high and low transmission regions accommodating many sharp resonance features. Here, we focus on the sharp resonance features for further analysis. The two features in regions A and B show vanishingly narrow resonance bandwidth as θ approaches 0° and 15.4°, respectively. These regions are magnified in Fig. 1c,d for clearer

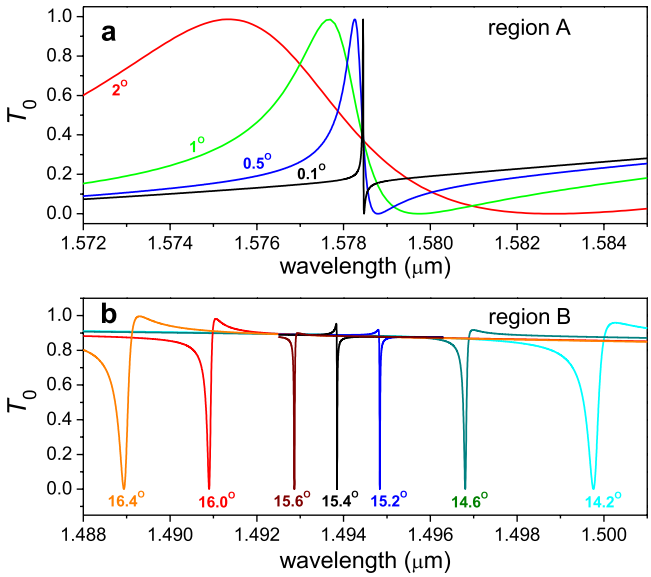

Figure 2. Spectral profiles of zero-order transmittance for several sampled angles of incidence in region A (**a**) and region B (**b**).

confirmation of the vanishing bandwidth. These high-Q resonance excitations produce extremely sharp spectral profiles as shown in Fig. 2. The resonance bandwidth approaches 2.9 fm for the region-A resonance and 9.2 pm for the region-B resonance. The corresponding resonance Q-factors are 5.46×10^8 and 1.62×10^5 for resonance in region A and B, respectively.

Internal field distributions reveal the nature of the modes inducing these high-Q resonances. The field distributions associated with the region-A resonance are shown in Fig. 3a–c when the field enhancement becomes maximal at $\lambda = 1578.547$ nm and $\theta = 0.00125°$. We will explain the reason why the field enhancement maximum occurs at this particular angle of incidence later in this paper. In these field distributions, we note that the electric field intensity $|\mathbf{E}|^2$ inside the Si ridges and their surfaces is enhanced by a factor exceeding 10^8. Hence this resonance excitation is highly desirable for surface-emitting Si-Raman amplifiers/lasers. In addition, it is of great interest to optimize the proposed device class in liquid environment for its application as efficient surface-enhanced Raman templates where at least 10^7–10^8 scale electric field enhancement factor is required for single-molecule-level detection sensitivity[18]. The field distributions show that each Si ridge excites a typical radiation patterns of a cylindrical electric dipole aligned with surface normal axis. The tangential field components (H_y and E_x) are anti-symmetric with respect to the mirror-symmetry plane of the structure, i.e., y-z plane in our case. Therefore, leakage radiation to the surface normal direction is forbidden because of symmetry incompatibility with the external radiation whose tangential field components are symmetric with respect to the mirror-symmetry plane. Leakage radiation to the off-normal direction is also forbidden due to the subwavelength periodicity. This property explains the vanishingly narrow resonance bandwidth of the region-A resonance as $\theta \to 0°$. This type of radiation decay suppression is also closely related to destructive interference between emitted radiation fields from two counter-propagating leaky guided modes for standing-wave conditions at either one of two edges of a stopband[19,20].

In contrast, the region B resonance is not explained by the mode's symmetry incompatibility with the external radiation fields or interference properties for standing-wave conditions because the resonance bandwidth vanishes for non-zero angle $\theta \to 15.4°$ and the incident fields are not necessarily symmetric or anti-symmetric with respect to the mirror-symmetry plane of the structure. Instead, the physical origin of the ultrahigh-Q resonance in region B is related to simultaneous suppression of the leakage radiation amplitudes to the zero-order waves in air cover and silica substrate. This effect involves interference between partial leakage radiations from different Bloch modes and complex interaction of evanescent fields at the top and bottom interfaces of the film[3,21]. The internal field distributions associated with the region B resonance are shown in Fig. 3d–f and we confirm the electric field intensity enhancement factor in the order of 10^5.

Resonance Q factors and field enhancement

Considering applications of high-Q resonances in periodic thin films to biochemical sensors, SERS templates, and nonlinear optical components, the resonance Q factor Q and associated field intensity enhancement factor W are important figures. We further investigate dependences of these parameters on the excitation condition and derive a useful relation between Q and W in the presence of material dissipation that is unavoidable due to internal absorption and diffuse scattering by film imperfections such as surface roughness, vacancies, and grain boundaries.

Following the conventional terminology, we define the total resonance Q factor $Q_{tot} \equiv \lambda_0/\Delta\lambda = \omega_0/2(\gamma_A + \gamma_R)$, where λ_0 is resonance center wavelength, $\Delta\lambda$ is full-width at half-maximum of the resonance, ω_0 is angular frequency of the resonance center, and γ_A and γ_R denote partial damping rates due to the material dissipation and leakage radiation, respectively. We also define partial resonance Q factors $Q_A \equiv \omega_0/2\gamma_A$ as dissipation Q factor and

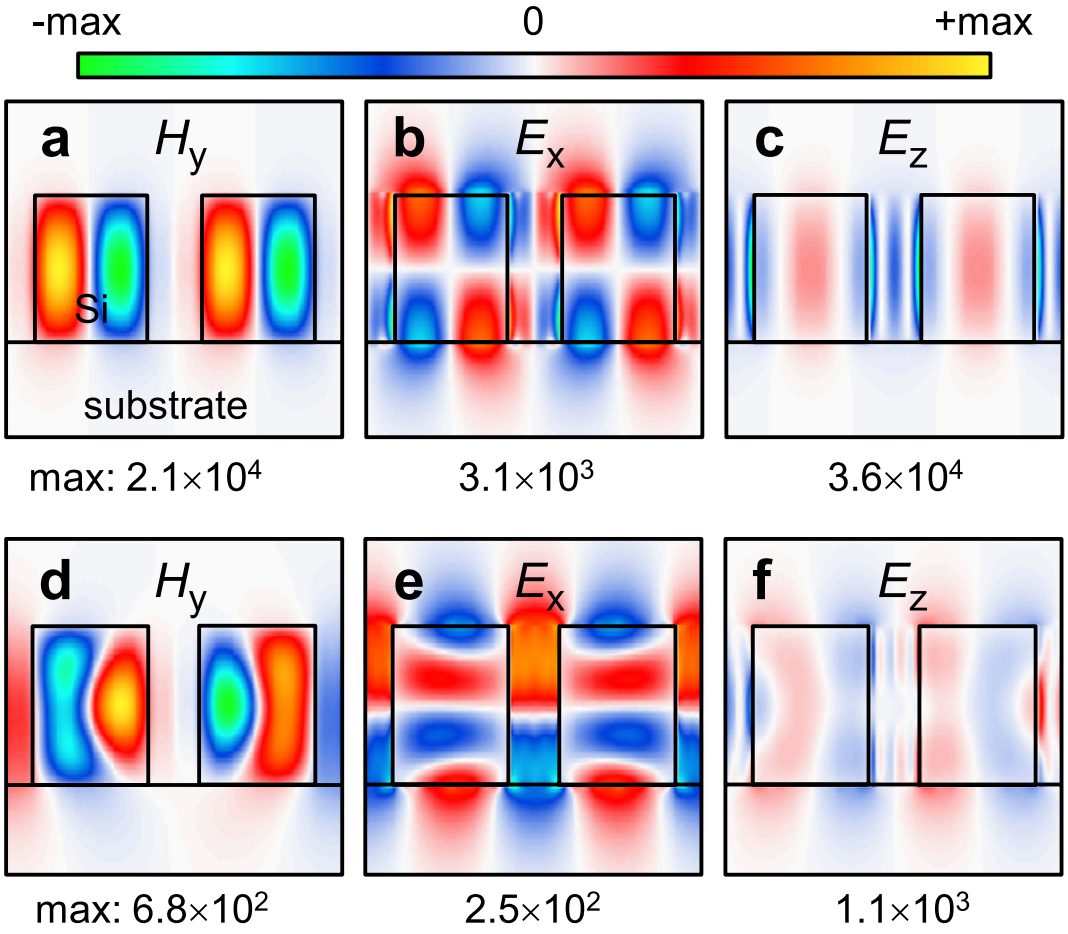

Figure 3. Field distributions associated with the high-Q resonance features in (**a–c**) region A and (**d–f**) region B. Corresponding wavelengths and angles of incidence are selected when the field enhancement becomes maximal. For (**a–c**), $\lambda = 1578.457$ nm and $\theta = 0.00125°$. For (**d–f**), $\lambda = 1493.849$ nm and $\theta = 15.4°$. Note H and E denote magnetic and electric field amplitudes, respectively, and the values are normalized by incident field amplitudes.

$Q_R \equiv \omega_0/2\gamma_R$ as radiation Q factor. The total and partial Q factors are related by $1/Q_{tot} = 1/Q_A + 1/Q_R$. For quantitative analysis of the field enhancement effect, we define two electric field intensity enhancement factors

$$W_v = \frac{\int_{\text{inside ridge}} |\mathbf{E}/E_0|^2 dV}{\int_{\text{inside ridge}} dV} \quad (1)$$

for the volume-average intensity inside the Si ridges and

$$W_s = \frac{\int_{\text{surface}} |\mathbf{E}/E_0|^2 dS}{\int_{\text{surface}} dS} \quad (2)$$

for the surface-average intensity on the surface exposed to the air, where **E** denotes electric field, E_0 is incident electric field amplitude, dV is infinitesimal volume, and dS is infinitesimal surface area. The two enhancement factors W_V and W_S are useful parameters in consideration of a resonance element as a nonlinear optical device using the film's native optical nonlinearity and a SERS template for molecular detection systems, respectively.

We estimate resonance Q factors Q_A, Q_R, and Q_{tot} and field enhancement factors W_V and W_S for our simulated cases as shown in Figs 4 and 5 for the region A and B resonances, respectively. For resonance Q factor estimation, we use the absorbance analysis method established in[22–24]. The field enhancement factors by the definition in Eqs. (1) and (2) are directly obtained from the calculated field distributions due to the rigorous coupled-wave analysis.

Figure 4a shows the dependences of Q_A, Q_R, and Q_{tot} on the angle of incidence θ for the region A resonance. The radiation Q factor Q_R is increasing with decreasing angle of incidence because of the symmetry incompatibility as discussed previously. In contrast, the dissipation Q factor Q_A is almost constant because the modal field distribution does not remarkably change the portion of field energy inside the Si ridges with the change in θ. Therefore, the total Q factor Q_{tot} increases with Q_R for the large angle-of-incidence range of $\theta > 0.01°$ and becomes saturated

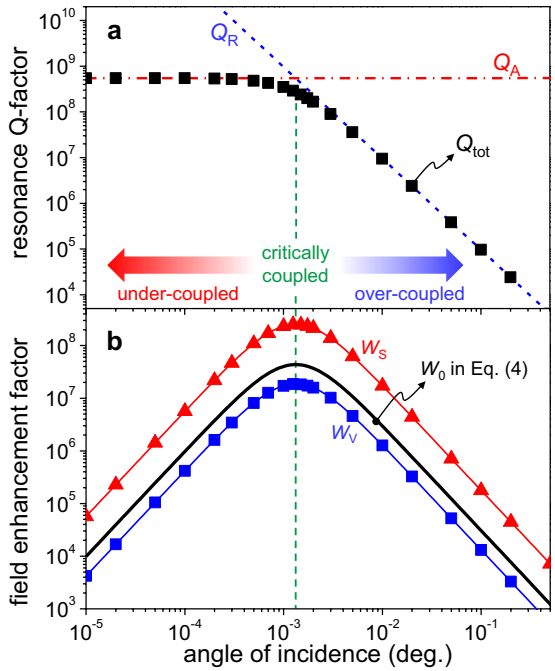

Figure 4. Field enhancement factors for critically coupled resonances in region A. (**a**) Partial and total resonance Q-factors. (**b**) Electric field intensity enhancement factors.

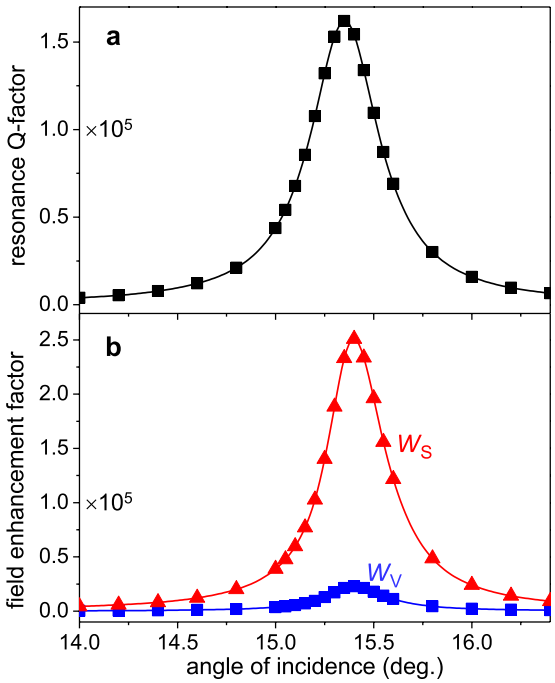

Figure 5. Field enhancement factors for over-coupled resonances in region B. (**a**) Total resonance Q-factor Q_{tot}. (**b**) Electric field intensity enhancement factors. Note that $Q_A = 4.2\sim4.4 \times 10^8$ is much higher than $Q_R \approx Q_{tot}$ in region B, implying that the region B resonances are highly over-coupled.

at $Q_A = 5.46 \times 10^8$ for the small angle-of-incidence range of $\theta < 0.001°$. Dependences of the field enhancement factors are quite distinguished from those of resonance Q factors as shown in Fig. 4b. Both W_V and W_S increase with increasing Q_{tot} for the large angle-of-incidence range of $\theta > 0.01°$, they are maximized at $\theta = 0.00125°$ where $Q_A = Q_R$, and they eventually show high slope decrease in the small angle-of-incidence range of $\theta < 0.001°$ although the total resonance Q factor is almost constant in this angle-of-incidence range.

We explain this non-trivial property of field enhancement factors on the basis of interference effects associated with generic optical Fano resonances. Using the coupled-mode theory of optical Fano resonances[23,25], the energy stored in the resonance mode at the resonance center is expressed by

$$U = \frac{1}{\pi}\eta_R(1 - \eta_R)Q_A C P_0 t_0, \tag{3}$$

where $\eta_R \equiv \gamma_R/(\gamma_A + \gamma_R) = Q_{tot}/Q_R$ is the radiation probability of the resonance mode, $C \equiv \gamma_1/\gamma_R$ with γ_1 denoting the partial radiation decay rate to the reflected wave is the relative strength of radiation coupling of the resonance mode with the reflected wave, P_0 is the power delivered by the incident wave, and $t_0 \equiv 2\pi/\omega_0$ is the optical cycle at the resonance center. According to the Lorentz reciprocity theorem for electromagnetic fields, the coupling strength constant C also can be interpreted as a relative coupling strength of the resonance mode with the incident wave. Field enhancement factors W_V and W_S are directly proportional to the ratio of the energy U stored in the resonance mode to the portion of the incoming energy CP_0t_0 coupled with the resonance mode for an optical cycle. Following this argument, we define a general field enhancement factor W_0 such that

$$W_0 = \frac{U}{CP_0t_0} = \frac{1}{\pi}\eta_R(1 - \eta_R)Q_A, \tag{4}$$

Equation (4) with the partial resonance Q factors Q_A and Q_R found in Fig. 4a quantitatively describes the dependence of W_V and W_S on the angle of incidence as shown in Fig. 4b.

It is obvious in Eq. (4) that the field enhancement does not simply increase with the total Q factor Q_{tot} but it has the maximum at the critical coupling condition where $\eta_R = 1/2$, or $Q_R = Q_A = 2Q_{tot}$ equivalently. This is a result of a well-known effect of destructive interference of the resonant and non-resonant pathways in the reflected and transmitted waves. At the critical coupling condition, the destructive interference becomes strongest because the two contributions of the resonant and non-resonant pathways to the outgoing waves have the same intensities with π phase difference. This intensity and phase property is dictated by the time-reversal symmetry of the wave coupling processes[22,23,25].

For under-coupled resonances with $\eta_R < 1/2$ and $Q_R > Q_A$, intensity of the resonant contribution is not strong enough to cancel the non-resonant contribution and hence the light trapping effect is not as strong as for the critically coupled resonances. Alternatively, the field enhancement for an under-coupled resonance does not reach its obtainable maximum with a given Q_{tot} because the rate of radiative energy coupling from the incident wave to the resonance mode is slower than the internal damping rate due to the material dissipation. For highly under-coupled resonances with $\eta_R \ll 1/2$ and $Q_R \gg Q_A$, Eq. (4) reduces to $W_0 \approx (Q_A/Q_R)Q_{tot}/\pi$. Therefore, the field enhancement is suppressed by a factor Q_A/Q_R ($\ll 1$) from that expected for lossless or highly over-coupled resonances. This explains the high-slope decrease of the field enhancement factors of the region A resonance without substantial decrease in Q_{tot} for the small angle-of-incidence range in Fig. 4b.

In the opposite cases of over-coupled resonances with $\eta_R > 1/2$ and $Q_R < Q_A$, the resonant contribution dominates the outgoing wave intensities over that from the non-resonant contribution and hence the trapping effect becomes weaker than that for the critically coupled resonances. Alternatively, an over-coupled resonance can be considered to have an excessive radiation decay that exhausts the localized energy before it reaches its maximum limit for a given amount of material dissipation. Equation (4) for the general field enhancement factor reduces to $W_0 \approx Q_{tot}/\pi$ for highly over-coupled resonances with $\eta_R \gg 1/2$ and $Q_R \ll Q_A$. Therefore, the field enhancement is simply proportional to the total Q factor. This explains the dependences of W_V and W_S on the angle of incidence for the region B resonance that is highly over coupled with $Q_A \gg Q_{tot} \approx Q_R$. Figure 5a,b show the estimated Q_{tot} and field enhancement factors as functions of angle of incidence. We confirm that the volume and surface field enhancement factors (W_V and W_S) are maximized at the angle of incidence corresponding to the Q_{tot} peak. Note that lossless cases is also considered as a highly over-coupled resonance because lossless resonances satisfy $Q_A = \infty \gg Q_R$.

Considering real experiments on ultrahigh-Q resonances and associated strong field enhancement, it is important to optimize the amount of the radiation damping of a resonance in accordance with the material dissipation of thin-film materials. High-index semiconductors, nitrides, and metal oxides such as Si, Ge, GaAs, $Si3N_4$, TiO_2, and HfO_2 are common materials for resonant thin-film devices. The intrinsic dissipation of these materials is unavoidable and highly dependent on the film deposition and lithographic etching conditions that determine grain size, density of vacancies, and surface roughness. In addition to the material's internal absorption, these film imperfections cause diffuse scattering that contributes to extinction coefficients in the order of $10^{-5} \sim 10^{-3}$ [26–28]. Therefore, in order to obtain the strong field enhancement effect, device parameters such as fill factor and modulation depth of the pattern that primarily determine the radiation damping rate of a resonance mode should be properly optimized to satisfy the critical coupling condition for a given level of material dissipation. This factor is even more important in nanostructured plasmonic resonance systems including surface plasmonic biochemical sensors and nonlinear plasmonic metamaterials[29,30]. In plasmonic metals including Ag, Au, Al, and Cu, the ohmic absorption is high in the optical frequency domain and dense surface charges induce strong light scattering even from deep-subwavelength rough features on their surfaces.

Conclusion

In conclusion, we address ultrahigh-Q resonances in a subwavelength Si grating. We show that a strongly modulated *c*-Si subwavelength grating supports embedded and quasi-embedded photonic bound states with resonance Q and field enhancement factors exceeding 10^8. We find that in the presence of material dissipation the field enhancement associated with an embedded photonic bound state is not simply proportional to the resonance Q factor because of a particular interference effect generally involved in the resonant light trapping effect. Using the coupled-mode theory of general optical Fano resonances, we derive an analytic expression of

the field enhancement factor in terms of the radiation probability and absorption Q factor of a bound state. We confirm quantitative agreement of this expression with rigorous numerical calculation results showing the field enhancement maximized at the critical condition where the radiation Q factor is identical to the absorption Q factor. Therefore, our results provide useful knowledge for designing practical resonance elements in various application areas including SERS-based molecular detection systems, cavity-QED problems, and nonlinear optical devices.

References

1. Von Neumann, J. & Wigner, E. Über merkwürdige diskrete Eigenwerte. *Phys. Z.* **30,** 465–467 (1929).
2. Marinica, D. C., Borisov, A. G. & Shabanov, S. V. Bound states in the continuum in photonics. *Phys. Rev. Lett.* **100,** 183902 (2008).
3. Hsu, C. W. *et al.* Observation of trapped light within the radiation continuum. *Nature* **449,** 188–191 (2013).
4. Silveirinha, M. G. Trapping light in open plasmonic nanostructures. *Phys. Rev. A* **89,** 023813 (2014).
5. Monticone, F. & Alù, A. Embedded photonic eigenvalues in 3D nanostructures. *Phys. Rev. Lett.* **122,** 213903 (2014).
6. Plotnik, Y. *et al.* Experimental observation of optical bound states in the continuum. *Phys. Rev. Lett.* **107,** 183901 (2011).
7. Lannebère, S. & Silveirinha, M. G. Optical meta-atom for localization of light with quantized energy. *arXiv:* **1509,** 008758v3 (2015).
8. Wang S. S. & Magnusson, R. Theory and applications of guided-mode resonance filters. *Appl. Opt.* **32(14),** 2606–2613 (1993).
9. Magnusson, R., Yoon, J. & Wawro, D. Properties of resonant modal-plasmonic multiparametric biosensors. *Proc. SPIE* **8570**, *Frontiers in Biological Detection: From Nanosensors to Systems V*, 85700K (2013), doi: 10.1117/12.2004550.
10. Ding, Y. & Magnusson, R. Resonant leaky-mode spectral-band engineering. *Opt. Express* **12,** 5661–5674 (2004).
11. Fattal, D., Li, J., Peng, Z., Fiorentino, M. & Beausoleil, R. G. Flat dielectric grating reflectors with focusing abilities. *Nat. Photon.* **4,** 466–470 (2010).
12. Lee, J. H. *et al.* A semiconductor metasurface with multiple functionalities: A polarizing beam splitter with simultaneous focusing ability. *Appl. Phys. Lett.* **104,** 233505 (2014).
13. Ginn, J. C. *et al.* Realizing optical magnetism from dielectric metamaterials. *Phys. Rev. Lett.* **108,** 097402 (2012).
14. Monticone, F. & Alù, A. Leaky-wave theory, techniques, and applications: From microwaves to visible frequencies. *Proc. IEEE* **103(5),** 793–821 (2015).
15. Collin, S. Nanostructure arrays in free-space: optical properties and applications. *Rep. Prog. Phys.* **77,** 126402 (2014).
16. Moharam, M. G., Grann, E. B., Pommet, D. A. & Gaylord, T. K. Formulation for stable and efficient implementation of the rigorous coupled-wave analysis of binary gratings. *J. Opt. Soc. Am. A* **12,** 1068–1076 (1995).
17. E. D. Palik, *Handbook of Optical Constants of Solids* (Academic Press, 1985).
18. Le Ru, E. C., Blackie, E., Meyer, M. & Etchegoin, P. G. Surface enhanced Raman scattering enhancement factors: A comprehensive study. *J. Phys. Chem. C* **111,** 13794–13803 (2007).
19. Kazarinov, R. F. & Henry, C. H. Second-order distributed feedback lasers with mode selection provided by first-order radiation losses. *IEEE J. Quantum Electron.* **QE-21**, 144–150 (1985).
20. Ding, Y. & Magnusson, R. Band gaps and leaky-wave effects in resonant photonic-crystal waveguides. *Opt. Express* **15,** 680–694 (2007).
21. Yang, Y., Peng, C., Liang, Y., Li, Z. & Noda, S. Analytical perspectives for bound states in the continuum in photonic crystal slabs. *Phys. Rev. Lett.* **113,** 037401 (2014).
22. Yoon, J. W., Jung, M. J., Song, S. H. & Magnusson, R. Analytic theory of the resonance properties of metallic nanoslit arrays. *IEEE J. Quantum. Electron.* **48,** 852–861 (2012).
23. Yoon, J., Seol, K. H., Song, S. H. & Magnusson, R. Critical coupling in dissipative surface-plasmon resonators with multiple ports. *Opt. Express* **18,** 25702–25711 (2010).
24. Yoon, J., Song, S. H. & Kim, J.-H. Extraction efficiency of highly confined surface plasmon-polaritons to far-field radiation: an upper limit. *Opt. Express* **16,** 1269–1279 (2008).
25. Fan, S., Suh, W. & Joannopoulos, J. D. Temporal coupled-mode theory for the Fano resonance in optical resonators. *J. Opt. Soc. Am. A* **20,** 569–572 (2003).
26. Amin, M. S., Hozhabri, N. & Magnusson, R. Effects of solid phase crystallization by rapid thermal annealing on the optical constants of sputtered amorphous silicon films. *Thin Solid Films* **545,** 840–484 (2013).
27. Liao, B.-H. & Hsiao, C.-N. Improving optical properties of silicon nitride films to be applied in the middle infrared optics by a combined high-power impulse/unbalanced magnetron sputtering deposition technique. *Appl. Opt.* **53,** A377–A382 (2014).
28. Rao, K. N. Influence of deposition parameters on optical properties of TiO_2 films. *Opt. Eng.* **41,** 2357–2364 (2002).
29. Piliarik, M. & Homola, J. Surface plasmon resonance (SPR) sensors: approaching their limits? *Opt. Express* **17,** 16505–16517 (2009).
30. Klein, M., Enkrich, C., Wegener, M. & Linden, S. Second-harmonic generation from magnetic metamaterials. *Science* **313,** 502–504 (2006).

Acknowledgements

This work was supported in part by the United States Air Force Office of Scientific Research under Agreement Number FA9550-10-1-0543, the Basic Science Research Program (NRF-2015R1A2A2A01007553), and by the Global Frontier Program through the National Research Foundation (NRF) of Korea funded by the Ministry of Science, ICT & Future Planning (NRF-2014M3A6B3063708). Additional support was provided by a UT System Texas Nanoelectronics Research Superiority Award funded by the State of Texas Emerging Technology Fund as well as by the Texas Instruments Distinguished University Chair in Nanoelectronics endowment.

Author Contributions

This research was planned by J.W.Y. Numerical simulation was performed by J.W.Y. The authors J.W.Y., S.H.S. and R.M. discussed the results. J.W.Y., S.H.S. and R.M. wrote the manuscript.

Additional Information

Competing financial interests: The authors declare no competing financial interests.

How to cite this article: Yoon, J. W. *et al.* Critical field enhancement of asymptotic optical bound states in the continuum. *Sci. Rep.* **5**, 18301; doi: 10.1038/srep18301 (2015).